SPECTROSCOPIC CHARACTERIZATION OF BINUCLEAR RUTHENIUM-OSMIUM COMPLEXES

By

JAIRED TATE

A THESIS PRESENTED TO THE GRADUATE SCHOOL
OF THE UNIVERSITY OF FLORIDA IN PARTIAL FULFILLMENT
OF THE REQUIREMENTS FOR THE DEGREE OF
MASTER OF SCIENCE

UNIVERSITY OF FLORIDA

2011

To the memory of my father, James Edward Tate, Jr.

ACKNOWLEDGMENTS

This thesis would be merely a dream without the support of countless individuals that I have encountered before and during this process. I credit any measure of success that I have achieved and any that I will receive to people in my life. Although I cannot possibly mention everyone, I would like to highlight a few individuals.

I would like to express my utmost appreciation to my advisor, Valeria Kleiman. Her seemingly infinite knowledge, patience, and willingness to develop others into scientists have set a standard for me that I would like to match some day. I also want to thank members of the Kleiman research group, both past and present, for creating an environment that was academically stimulating, yet, warm and friendly. Shiori Yamazaki has been especially helpful in helping me understand the transient absorption experiment, so thanks a bunch.

Additionally, I would like to thank my committee members for their willingness to serve on my committee. I realize that they each have other commitments that require their time and energy, yet, you agreed to be a part of this part of my graduate experience and for that, I am grateful.

I also want to thank the Office of Graduate Minority Programs (OGMP) at the University of Florida. OGMP has allowed me to learn about and receive the NSF Bridge to Doctorate Fellowship and the FAMU Feeder Fellowship , as well as serve as a place for encouragement while I have been at this school, for which I am truly thankful.

Last, but certainly not least, I would like to thank my family. My parents have spared nothing from me that they felt would benefit me and I am forever grateful. I thank my mom for pushing me to always try to do my absolute best, for encouraging me to build a strong relationship with God, and loving me unconditionally. Although my dad

passed away shortly after I began this program, I will always remember that he would constantly remind me that I can do anything that I truly put my mind to. I thank my beautiful wife Tia for being so loving and supportive, and for understanding that much of our quality time has been sacrificed for my time in the lab. I also thank my son, Jaired Jr. (JJ), whom I love more than can ever be expressed with mere words for just being here and giving me those smiles for renewed motivation, and those cries that have kept me up some nights.

TABLE OF CONTENTS

page

LIST OF TABLES

LIST OF FIGURES

LIST OF ABBREVIATIONS

BBO	barium borate
bpy	2,2’-bipyridine
DSSC	Dye-sensitized solar cell
FHG	fourth harmonic generation
fs	femtosecond
FWHM	full width at half maximum
LMCT	ligand to metal charge transfer
MLCT	metal to ligand charge transfer
MMCT	metal to metal charge transfer
ns	nanosecond
OD	optical density
OPA	optical parametric amplifier
ps	picosecond
SHG	second harmonic generation
tpm	tris(1-pyraxolyl)methane
TPP	tetraphenylphosphonium
tpy	2,2’:6’:2’-terpyridine
UV	ultraviolet
Vis	visible

Abstract of Thesis Presented to the Graduate School
of the University of Florida in Partial Fulfillment of the
Requirements for the Degree of Master of Science

SPECTROSCOPIC CHARACTERIZATION OF BINUCLEAR RUTHENIUM-OSMIUM COMPLEXES

By

Jaired Tate

December 2011

Chair: Valeria Kleiman
Major: Chemistry

Transition metal complexes have garnered much attention recently for their potential use in light harvesting processes. One of the fundamental processes that makes them attractive is electron transfer. In this thesis, a series of binuclear complexes consisting of a ruthenium center and an osmium center have undergone spectroscopic experiments. The tridentate terminal ligand of the ruthenium and the oxidation state of the osmium were varied to determine how these properties mediate electron transfer properties. The results from steady state as well as time-resolved studies are presented herein. Also contained in this thesis are proposed experimental modifications to improve future experiments.

CHAPTER 1
BACKGROUND AND OVERVIEW

1.1-Energy Demand

It is a well-known fact that society is in the midst of an energy crisis.[1] This is primarily due to our consumption of fossil fuels, which are non-renewable. The rapid rate of energy usage dictates that these resources will be used up in the near future. Projections predict that energy demands in the United States will increase 33% for oil and 62% for natural gas by 2020.[2] In addition to this, the fossil fuels have an adverse effect on the environment. In the United States, over 90% of greenhouse gases come from fossil fuel combustion. [3] Consequently, there is increased interest in finding an alternate source of energy that is both renewable and safe for the environment.

One source of alternate energy that has been of interest to researchers is solar energy. The amount of solar energy to reach Earth's surface in an hour is approximately equal to the amount of fossil fuels used by our planet in a year.[4] Thus, if there was a way to harvest this energy and efficiently convert it to a form of useful chemical energy, our demand for energy could be met better. One way of approaching this issue is by studying photosynthetic processes, in which plants and algae convert energy from the sun into chemical energy needed to survive.

In photosynthesis, chlorophylls absorb photons from the sun. The resulting excited chlorophylls transfer electrons to an initial electron acceptor, quinone, and subsequently, to a final electron acceptor.[5] As a result of the series of electron transfer steps, a charge-separated state is created. The energy of the charge-separated state is used for the reactions of photosynthesis[6] , which results in formation of O_2 and glucose. The glucose molecules store chemical energy in their bonds. Since photosynthesis is a

means of converting solar energy into chemical energy without harmful byproducts, researchers have an interest in harnessing sunlight for energy demands. One approach is to mimic essential events of photosynthesis in order to directly get energy conversion.

1.2- Dye Sensitized Solar Cells

Michael Grätzel revolutionized th**e** field of light harvesting by introducing the dye-sensitized solar cell (DSSC). DSSCs consist of a nanocrystalline network of a semiconductor with wide band gap energy (most commonly, TiO_2), a layer of dye molecules, a redox electrolyte, and a counter electrode.[7] Upon light absorption, the dye is promoted to an excited state, followed by electron injection into the semiconductor material, and electron diffusion through the film; the dye is regenerated via electron transfer from the electrolyte.[7, 8] The charge separation exhibited by the dye is a key process, and occurs on an ultrafast timescale.

In recent years, the desire to make better DSSCs has been approached by examining photophysical properties of dyes made of transition metal complexes that absorb light and subsequently undergo electron transfer. Researchers interested in understanding factors that mediate the chemistry at these metal centers have been directed by structural and mechanistic knowledge obtained by research on natural photosynthetic centers.[9] Target model complexes should exhibit: (i) photochemical stability; (ii) strong absorption in the visible region; (iii) an electron donor and an electron acceptor properties; (iv) a long-lived charge separated state.[10] $[Ru(bpy)_3]^{n+}$ is a dye that has been used extensively in DSSCs as it possesses desired characteristics.[11]

1.3- Ru(bpy)3

Tris(bipyridine)ruthenium(II) ($[Ru(bpy)_3]^{n+}$ has been studied extensively for its potential for use in light harvesting. It has an unusual combination of stability, desirable

redox properties, long lived excited state and excited state reactivity.[12] It exhibits broadband absorption, absorbing in the ultraviolet and visible regions. A number of spectroscopic techniques have been used extensively to understand the photophysics, photochemistry, energy transfer and electron transfer in $Ru(bpy)_3]^{n+}$.[13] Upon excitation with visible light, an electron is promoted from the metal to a bipyridine orbital. It has been shown that the electron is localized on one of the bipyridine ligands in ~60 fs.[14] Following this, a conversion from the singlet excited state to a triplet excited state occurs with a quantum yield near unity in ~100 fs. [15, 16] The excited state relaxes radiatively to the ground state with a lifetime ~600 ns in aqueous solution. [17, 18]

The wealth of knowledge obtained from $[Ru(bpy)_3]^{n+}$ has caused researchers to use the complex as a precursor to other molecules/complexes by attaching other ligands and/or other metals to the $[Ru(bpy)_3]^{n+}$ core.[19-27] Interest lies in tuning the electronic properties, including the electronic region of absorption, the excited state lifetime, and the electron transfer distance.[28] By doing so, conclusions are drawn regarding structural influences on ground and excited state behavior in the complexes. For example, in one study by Turro and coworkers, quinolate derivatives were used as ligands to make analogs to $Ru(bpy)_3$.[29] It was found that the lowest energy transition occurs from an orbital not purely metal centered, unlike the transition in $[Ru(bpy)_3]^{n+}$. One class of compounds that are of interest is bimetallic complexes (dimers), which contain two metal centers covalently attached by a bridging ligand.[30, 31] Bimetallic complexes are attractive in light harvesting research because the conversion of solar energy into useful chemical energy, the absorbing entity needs to transfer energy or an electron to another entity.[32] The combination of more than one metal center offers

greater flexibility in terms of absorption and excited state energy when compared to the mononuclear counterparts.[33] The attachment of a metal center to the absorber may add additional relaxation pathways for the excited state and promote effective charge separation.[34] Additionally, binuclear complexes can be favored over mononuclear complexes as they can have well defined molecular lengths and contribute understanding to fundamental interfacial electron transfer.[35, 36]

Mixed valence dimers contain two metal centers with different oxidation states and are attractive due to their potential for inner-sphere electron transfer between two metal centers, known as an intervalence transition, or a metal to metal charge transfer (MMCT).[37] Robin and Day introduced a classification system for mixed valence dimers: [38] class I- negligible coupling between metal centers; class II- weak coupling between metal centers and; class III- strong coupling between the metal centers.[39] In the class I mixed valence complexes, the electronic coupling between the metal centers is nonexistent, such that the mixed valence complex exhibits properties of the individual monomeric species. In the class II mixed valence complexes, there is a small degree of electronic coupling such that the mixed valence complex exhibits characteristics not connected to the monomeric species. In class III mixed valence complexes, the degree of electronic communication is significant, such that the properties of the monomeric species are absent and new properties are observed.[40] The degree of coupling is dictated by the terminal ligand, bridging ligand, and metal character .[41, 42]

1.4- This Work

The goal of this project is to understand how structural components mediate electron transfer. This thesis examines spectroscopic properties of binuclear ruthenium-osmium complexes: K_2[RuII(tpy)(bpy)(NC)OsII$(CN)_5$] ($Ru^{II}(tpy)Os^{II}$),

TPP[RuII(tpy)(bpy)(NC)OsIII(CN)$_5$] ($Ru^{II}(tpy)Os^{III}$); and TPP[RuII(tpm)(bpy)(NC)OsIII(CN)$_5$] ($Ru^{II}(tpm)Os^{III}$), where tpy is the 2,2';6',2"-terpyridine ligand, tpm is the tris(1-pyrazolyl)methane ligand, and TPP is the counter ion tetraphenylphosphonium. (see Figure 1-4 for their structures) Both, tpy and tpm, are tridentate ligands, binding at three sites on the metal (Figure 1-5). The tpy ligand is known to form linear complexes with the metal center.[43] In tpy complexes, the bpy ligand is parallel with respect to the intermetallic (Ru-CN-Os) axis. The tpm ligand is coordinated to the metal in the fac configuration,[44] such that the ligand is orthogonal to the metal. The bpy ligand is perpendicular to the intermetallic axis in complexes with the tpm ligand. The cyano- group has been shown to bridge two metal centers in a linear arrangement stabilizing various oxidation states of transition metals.[45] Complexes $Ru^{II}(tpy)Os^{III}$ and $Ru^{II}(tpm)Os^{III}$ are mixed valence species, as they contain metal centers with two different oxidation states.

As a primary step we would like to characterize the photophysical properties of these bimetallic complexes, and to do so, we will utilize various spectroscopic methods. Steady state methods employed will include UV-Vis absorption spectroscopy and fluorescence emission spectroscopy. Femtosecond transient absorption spectroscopy will also be used to reveal excited state lifetimes and the presence of transients on the systems. The data will be interpreted in a manner to give insight into how the presence of osmium mediates excited state properties of the system by comparing results to studies done previously in this lab on ruthenium monomers with the tpy and tpm ligands as well as with osmium monomer properties from the literature.

1.5- Metal complex electronic transitions

Absorption in the ultraviolet (UV) and visible (Vis) regions of the electromagnetic spectrum is induced when a sample is irradiated with photon energy resonant to a transition. This results in valence electrons being promoted to a state of higher energy. One class of transitions is charge transfer. If electrons move from an orbital predominately ligand in character to an orbital predominately metal in character, it is classified as a ligand-to-metal charge-transfer (LMCT) transition; if the electron moves from an orbital predominately metal in character to an orbital predominately ligand in character, it is classified as a metal-to-ligand charge-transfer (MLCT) transition.[46] Once in an electronically excited state, molecules have various ways of relaxation. There may be relaxation between vibrational levels by the release of heat and collisions with solvent molecules in a process known as vibrational relaxation. There may also be relaxation between electronic levels, in a process known as internal conversion. The molecule may go from a spin-paired singlet state to a spin unpaired triplet state in a process called intersystem crossing. There are also radiative processes in which the molecule gives off excess energy as light. If light is emitted from a singlet state, the process is fluorescence; if the light emission is from a triplet state, it is phosphorescence. Transition metal complexes may also undergo bimolecular processes while in the excited state. One of these processes is electron transfer, after which, a charge-separated state may be created.

Electron transfer is essentially the transfer of an electron from a donor site, D, to an acceptor site, A. Two main mechanisms by which the electron transfer occurs are photoinduced electron transfer and optical electron transfer. Photoinduced electron

transfer involves a thermal reaction from a locally excited state[47], and can be expressed as

$$D + A + h\nu \rightarrow D^* + A \quad (1\text{-}1)$$

$$D^* + A \rightarrow D^+ + A^- \quad (1\text{-}2)$$

In optical electron transfer, the electron directly moves from the donor to the acceptor[48], such that

$$D + A + h\nu \rightarrow D^+ + A^- \quad (1\text{-}3)$$

Electron transfer in solution is governed by Marcus Theory, which states that the rate of electron transfer (k_{ET}) can be described by

$$k_{ET} = \nu_n k e^{-(\frac{\Delta G^*}{RT})} \quad (1\text{-}4)$$

where ν_n is a nuclear frequency factor, k is an electronic transmission coefficient, and ΔG^* is the free energy of activation.[48] The k_{ET} is determined experimentally from transient absorption experiments by fitting the decay (or rise) signal to a sum of exponentials. The ΔG^* term allows for determination of thermal parameters for electron transfer[39] and is given by

$$\Delta G^* = (\frac{\lambda}{4})(1 + \frac{\Delta G^*}{\lambda})^2 \quad (1\text{-}4)$$

where λ is the reorganization energy and ΔG^o is the standard free energy change. The reorganization energy parameter is the sum of an inner contribution, λ_ι, which involves orientation of bond lengths and angles, and λ_o, which involves reorientation of the solvent molecules.

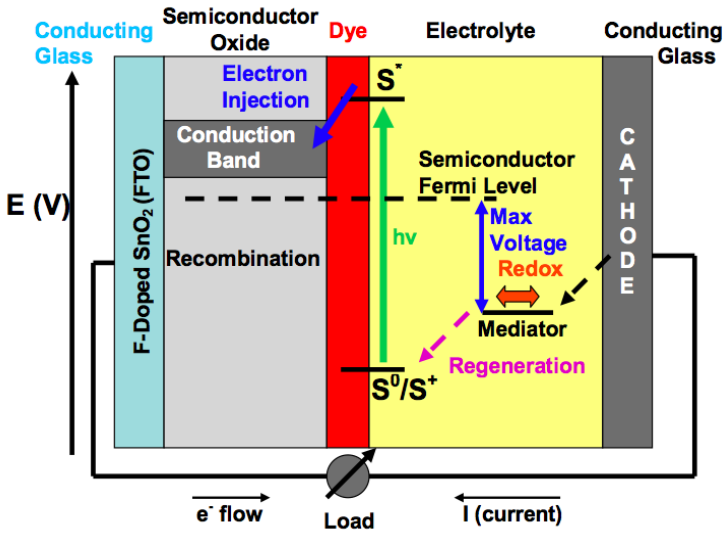

Figure 1-1. Schematic representation of a DSSC.

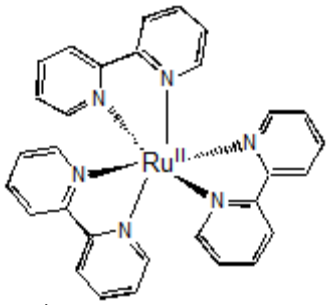

Figure 1-2. Structure of $[Ru(bpy)3]^{n+}$

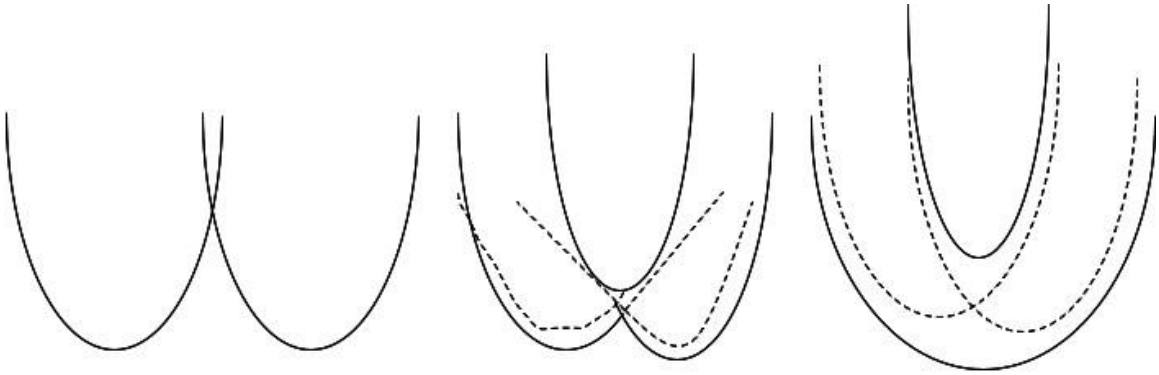

Figure 1-3. Potential energy curves for class I (left), class II (middle) and class III (right) mixed valence complexes. The solid curves represent adiabatic surfaces and the dotted curves represent diabatic surfaces. Figure adapted from literature source.[49]

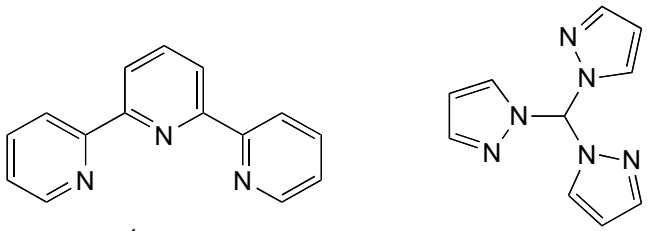

tpy tpm

Figure 1-4. Structures the tridentate ligands used in the complexes.

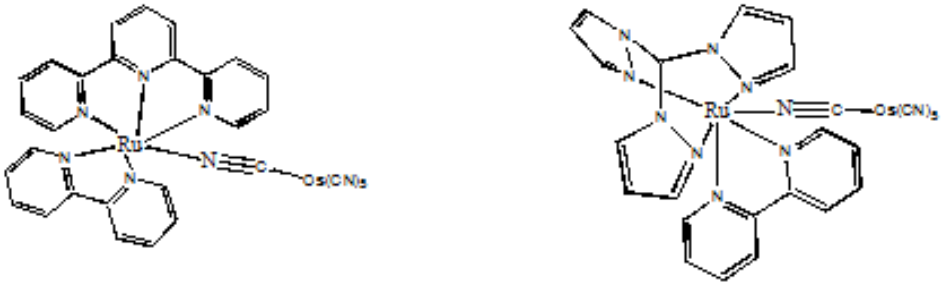

Figure 1-5. Structures of $Ru^{II}(tpy)Os^{II}$ and $Ru^{II}(tpy)Os^{III}$ (left) and $Ru^{II}(tpm)Os^{III}$ (right). In $Ru^{II}(tpy)Os^{II}$, the oxidation state of the osmium is II and in $Ru^{II}(tpy)Os^{III}$ and $Ru^{II}(tpm)Os^{III}$, the oxidation state of osmium is III.

CHAPTER 2
EXPERIMENTAL METHODS

Samples of $Ru^{II}(tpy)Os^{II}$ $Ru^{II}(tpy)Os^{III}$, and $Ru^{II}(tpm)Os^{III}$ were obtained through a collaboration with the research group of Professor Baraldo from of the University of Buenos Aires. Samples of $Ru^{II}(tpy)Os^{III}$ and $Ru^{II}(tpm)Os^{III}$, which contained the TPP counter ion were dissolved in anhydrous acetonitrile, whereas $Ru^{II}(tpy)Os^{II}$ was dissolved in distilled water.

2.1- Steady State Experiments

Absorption and fluorescence measurements were done in the materials chemistry characterization lab (MCCL) at the University of Florida. UV-Vis absorption data was collected using a Perkin Elmer Lambda 25 spectrophotometer. The instrument has a tungsten lamp for visible wavelengths and a deuterium lamp as its light source in the ultraviolet region. The detection range for these experiments was 300-800 nm. Fluorescence emission was accomplished using a Jobin-Jvon Spex-Fluorolog-3 fluorescence spectrometer, which uses a Xenon arc lamp as the light source, has an excitation range of 250-600 nm, and a detection range of 300-850 nm . The optical density of each sample was ~0.3 at the excitation wavelength. The emission experiments were done in right angle detection mode to minimize the effects of stray light. A 1 cm quartz cuvette was used for all experiments, and all experiments were performed at room temperature.

2.2- Ultrafast Transient Absorption Experiments

Transient absorption spectroscopy is a technique to monitor excited state processes. The use of short laser pulses allows for detection of lifetimes of species having short lifetimes. A femtosecond laser pulse is divided by a beam splitter into a

pump beam and a probe beam. The probe beam is further divided into a probe beam and a reference beam, to compensate for laser fluctuations. The higher intensity, monochromatic pump pulse excites a volume of the sample and the probe pulse, a white light continuum with lower intensity, monitors excited state changes after a specific delay time as a change in absorption. The absorption, A, can be expressed as:

$$A = -\log\left(\frac{I}{I_0}\right) = -\log T \tag{2-1}$$

where I is intensity of light in the presence of absorbing molecules, I_0 is intensity of light in the absence of absorbers, and T represents transmittance. After pump pulse excitation, the change in absorption (ΔA) is:

$$\Delta A(\lambda, \Delta t) = A_{pump\ on}(\lambda, \Delta t) - A_{pump\ off}(\lambda, \Delta t) \tag{2-2}$$

The change in absorption can be represented by the transmitted light to the detector, where the transmittance of the beams are the ratios of the intensity of the probe, which examines the excited sample volume, to the reference, which examines a volume of sample not excited by the pump. The relative change in transmittance, ΔT/T is:

$$\frac{\Delta T}{T} = \frac{T_{pump\ on} - T_{pump\ off}}{T_{pump\ off}} = \frac{\left(\frac{I_{t,probe}}{I_{ref}}\right)_{pump\ on} - \left(\frac{I_{t,probe}}{I_{ref}}\right)_{pump\ off}}{\left(\frac{I_{t,probe}}{I_{ref}}\right)_{pump\ off}} \tag{2-3}$$

In the equation above, pump on represents conditions when the pump beam is allowed to interact with the sample, pump off represents conditions when the pump beam is blocked by a mechanical chopper, I_{probe} represents probe beam intensity, and I_{ref} represents reference beam intensity.

There are generally contributions from a number of processes on a $\Delta T/T$ spectrum. The first is a ground state bleach, arising from the pump pulse exciting some of the ground state population. As a result, less molecules are in the ground state and more light gets to the detector, resulting in a positive signal. Another contribution to the $\Delta T/T$ spectrum is stimulated emission. This results when a photon from the probe pulse induces emission of another photon to the ground state from the molecule in the excited state.[50] The result is more light to the detector, hence, a positive signal. Additionally, a $\Delta T/T$ spectrum may contain contributions from excited state absorption. This is caused by absorption of the probe pulse in the excited state due to allowed transitions, resulting in a negative signal.

At a particular wavelength, the relaxation can be fit to an exponential model of the form

$$\Delta A = \sum_{n=1}^{n} A_n e^{-(\frac{t}{\tau_n})} \qquad (2\text{-}4)$$

A commercially available system from Spectra Physics was used to obtain ultrashort (~60 fs) laser pulses. The output of a cw Nd:YVO_4 laser (Millenia) gives a 532 nm beam. This output is used to pump a mode-locked Ti:sapphire laser (Tsunami), which produces pulses centered at 790 nm with ~35 nm (FWHM) bandwidth and ~35 fs in time at 82 MHz repetition rate. These pulses are used to seed a regenerative amplifier (Spitfire). The Spitfire is pumped by a Q-switched Nd:YLF laser (Evolution) which produces 532 nm pulses at 6.2 W and a repetition rate of 1 kHz. The Spitfire stretches, amplifies, and then compresses the pulses, giving an output with 790 nm pulses with 820 mW of power. The output of the Spitfire is split by a beamsplitter, as a

portion is used for white light generation and the rest is used to seed an optical parametric amplifier (OPA) for wavelength tunability.

The OPA utilizes a three-wave interaction process to derive its gain. For these types of processes, a continuum white light beam seeds a barium borate (BBO) crystal, and by correctly choosing the signal or idler beam, polarization, phase matching, and the number of harmonic crystals, a beam with wavelengths from ~300 nm to ~10 μm may be obtained.[51] For the experiments in this work, fourth harmonic (FHG) of the idler was generated by using two BBO crystals, and was used to generate pump pulses for the desired wavelengths

The output from the OPA passes through a telescope consisting of a convex lens (focal length=150 mm) and a concave lens (focal length=-50 mm) so that the beam is collimated. It then goes through an optical delay stage containing two mirrors on a translation stage, which is used to vary the delay between the pump and probe pulses at the sample position. After this, the beam goes through a mechanical chopper set to run at a frequency of 6.97 Hz to allow for "pump on" (pump beam transmitted) and "pump off" (pump beam blocked) conditions. Next, the beam is reflected off of a parabolic mirror (focal length= 152.4 mm), after which it is focused onto the sample and blocked after passing through the sample. The pump beam wavelengths used in this study were 415 nm, 435 nm, 460 nm, 480 nm, with pulse energies of 250 nJ, 600 nJ, 350 nJ, and 275 nJ, respectively.

A portion of the 790 beam that bypasses the OPA is used to generate a white light continuum by being focused onto a CaF_2 plate. The CaF_2 plate is housed in a mount and rotated in order to prevent degradation of the CaF_2. The white light is reflected off a

parabolic mirror then onto a beamsplitter to make the probe and reference beams. The beams travel to another parabolic mirror where they are then focused onto the sample, where the probe beam is overlapped with the pump beam. Temporal overlap is achieved by placing a nonlinear crystal at the sample position and translating the delay stage horizontally until a sum-frequency generation signal is detected by a photomultiplier tube. Spatial overlap is achieved by transmitting both beams through a pinhole at the sample position.

After the sample, the probe and reference beams are focused on a 150 mm slit on an Andor Shamrock spectrograph with a focal length of 303 mm. A grating blazed at 500 nm with a groove density of 150 lines/mm and a spectral range of 350-1050 nm is used to disperse the pump and probe beams. The spectral range of detection used here, limited by CaF_2, is 350-750 nm. The counts of the dispersed light are detected by an Andor iStar iCCD camera, which has an imaging area of 1024 rows x 256 columns of pixels. The change in transmitted light detected by the camera is monitored by a computer using a series of homemade LabVIEW® programs. One LabVIEW® program uses Equation 2-3 to generate a difference spectrum from the transmitted light by detecting the light in “pump on” and “pump off” conditions at different points in time (timesteps). Other LabVIEW® programs were used to control the position of the delay stage, the number of scans,** and the number of averages at each time step for each scan. Each experiment was done with at least 30 averages at each time step and at least 50 scans per experiment.

** I define a scan as a cycle through each of the selected timesteps.

All samples for transient absorption experiments were held in a 2-mm quartz cuvette, capped with a rubber septum, and degassed under argon for 15 minutes. The optical density of each sample was kept between 0.5 and 0.8 at the excitation wavelength. Photodegradation of the samples was monitored by taking the absorption spectrum of each before and after the transient absorption experiments.

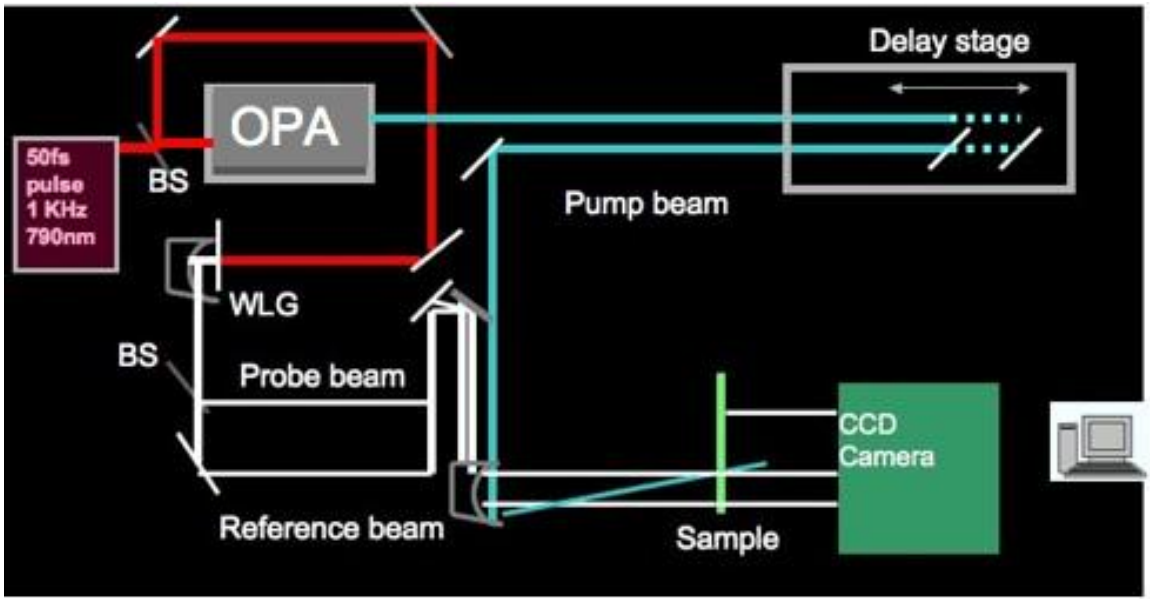

Figure 2-1. General schematic of the Transient Absorption setup.

CHAPTER 3
RESULTS AND DISCUSSION

3.1- Steady-State Measurements

The absorption spectrum for $Ru^{II}(tpy)Os^{II}$ in water can be seen in Figure 3-1 and is plotted with the $[Ru(II)(tpy)(bpy)CN]^{+}$ monomer in water. Both exhibit a broad absorption band in the visible region with a small shoulder (at 435 nm $Ru^{II}(tpy)Os^{II}$ and at 426 nm for the $[Ru(II)(tpy)(bpy)CN]^{+}$ monomer) at the blue edge of the band. This absorption band is typical in $[Ru(bpy)]^{2+}$ type complexes and assigned to a ^{1}MLCT absorption. The lower energy peak is attributed to an electron promoted from a ruthenium d-orbital to a tpy π^* orbital, while the shoulder is attributed to an electron promoted from a ruthenium d-orbital to a bpy π^* orbital. $Ru^{II}(tpy)Os^{II}$ also has an observable shoulder on the low energy end of the spectrum at wavelengths greater than 600 nm that extends beyond 800 nm , attributed to a normally forbidden transition that is allowed. Also observed is a red shift of the MLCT transition $Ru^{II}(tpy)Os^{II}$ with respect to the ruthenium monomer, as the absorption maximum is 483 nm for $Ru^{II}(tpy)Os^{II}$ and 460 nm for the monomer, attributed to the destabilization of the ruthenium d orbitals upon formation of the dimer, therefore decreasing the $d \rightarrow \pi^*$ gap.

The absorption spectrum for $Ru^{II}(tpy)Os^{III}$ in acetonitrile can be seen in Figure 3-2 and is plotted with the $[Ru(II)(tpy)(bpy)CN]^{+}$ monomer in acetonitrile. The ^{1}MLCT transition is seen for each complex, centered at 479 nm for $Ru^{II}(tpy)Os^{III}$ while the ruthenium monomer is slightly red-shifted with the MLCT peak intensity occurring at 485 nm. The $[Os(CN)6]^{3-}$ was not available for comparison at the time of this study, but information in the literature [52] of hexacyanoosmate (III) in acetonitrile reveals peaks in the absorption spectrum at 307 nm, 333 nm, and 400 nm, attributed to osmium d-orbital

to a cyanide π^* transitions, with the lowest energy band ending at 440 nm. In figure 3-2, a band is observable for $Ru^{II}(tpy)Os^{III}$ from 600 nm to 850 nm with peak intensity at 725 nm that is not observed in the ruthenium monomer, nor in the $Ru^{II}(tpy)Os^{II}$, which contains two metal centers with the +2 oxidation state. This is assigned to a $Ru^{2+} \rightarrow Os^{3+}$ MMCT transition.

The absorption spectrum for $Ru^{II}(tpm)Os^{III}$, in acetonitrile can be seen in Figure 3-3 and is plotted with the $[Ru(II)(tpm)(bpy)CN]^{+}$monomer in acetonitrile. The ^{1}MLCT transition is seen for both samples. . The monomer has peaks at centered at 417 nm for $Ru^{II}(tpm)Os^{III}$ and 433 nm which are assigned to ruthenium to bpy transitions, as transitions to the tpm ligand are expected to occur in the UV region.[53] A band is observable for $Ru^{II}(tpm)Os^{III}$ beginning just below 600 ad extending beyond 900 nm, centered around 850 nm. This is assigned to a $Ru^{2+} \rightarrow Os^{3+}$ MMCT transition.

Fluorescence emission measurements were done on the complexes in the same solvents from the absorption measurements. The emission spectra for the monomer, and $Ru^{II}(tpy)Os^{II}$, $Ru^{II}(tpy)Os^{III}$, and $Ru^{II}(tpm)Os^{III}$ are shown in Figure 3-4. The samples were excited at 480 nm and had an OD of ~ 0.3 at the excitation wavelength. The monomer and $Ru^{II}(tpy)Os^{II}$ both exhibit a broad featureless band originating at 600 and 650 nm, respectively, with a bandwidth of approximately 200 nm. The intensity of the emission in $Ru^{II}(tpy)Os^{II}$, however, is less than that of the monomer, and the emission intensities $Ru^{II}(tpy)Os^{III}$ and $Ru^{II}(tpm)Os^{III}$ are negligible in comparison. This result indicates that the presence of osmium causes emission to be quenched in these systems.

3.2- Time-Resolved Measurements

For the transient absorption experiments, the samples were excited in the MLCT bands. A portion of the spectra attributed to scatter from the pump has been removed in each figure. Additionally, the spectra exhibit a baseline shift (to be addressed in the following chapter). Because of this, the positive and negative signals that will be described refer to the concavity of the signals, where a concave down signal will be called positive and a concave up signal will be called negative. For the [Ru(II)(tpy)(bpy)CN] monomer in water, the transient absorption spectra following excitation at 460 nm ($Ru^{II} \rightarrow$tpy) and 435 nm ($Ru^{II} \rightarrow$bpy) can be seen in Figures 3-5 and 3-6, respectively. The spectra exhibit a negative signal attributed to excited state absorption from 340-400 nm and a positive signal attributed to a ground state bleach from 400-500 nm. The bleach signal is associated with the oxidation of the Ru(II) unit, and the excited state absorption is associated with the formation of the excited ligand radical.[54, 55] Both of these signals are seen beginning at time zero, formed by 200 fs and persist with no further spectral changes throughout the 20 ps time window, indicating that the complex has relaxed to the ^{3}MLCT state when excited at 460 nm. When excited using435 nm light, the bleach and the excited state absorption signal are seen beginning at time zero and are formed within 300 fs, with no major spectral changes throughout the 20 ps time window.

For Ru^{II}(tpy)Os^{II}, the transient absorption spectra following excitation at 480 nm and 435 nm can be seen in Figures 3-7 and 3-8, respectively with time delays up to 20 ps. When excited at 480 nm, Ru^{II}(tpy)Os^{II} a bleach is observable from 440-550 nm associated with oxidation of the Ru(II) center at time zero. The signal is formed within

200 fs, and persists for the duration of the 20 ps window with no apparent spectral changes. The sample also exhibits a decrease in transmission attributed to excited state absorption from 360-410 nm on the same time scale as the bleach signal. There is also a negative signal seen at wavelengths >550 nm corresponding to excited state absorption.

When $Ru^{II}(tpy)Os^{II}$ is excited using 435 nm light, a negative excited state absorption signal centered around 380 nm and a positive bleach signal centered around 500 nm are observed beginning at time zero and evolve until 500 fs, after which, no further significant spectral evolution is observed in the 20 ps window. A negative signal is observed at long wavelengths corresponding to excited state absorption.

Excitation pulses of 415 nm and 435 nm were used to excite $Ru^{II}(tpy)Os^{III}$. Excitation beams with central wavelength at 435 nm and 460 nm were used to excite $Ru^{II}(tpm)Os^{III}$. No transient signals were detected for $Ru^{II}(tpy)Os^{III}$ or $Ru^{II}(tpm)Os^{III}$. This is most likely due to experimental conditions, and will be addressed in more detail in the following chapter.

3.3- Discussion

In order to assess the role of the terminal tridentate ligand (tpy vs. tpm), differences in the electronic absorption spectrum of $Ru^{II}(tpm)Os^{III}$, which contains tpm, to that of $Ru^{II}(tpy)Os^{III}$, which contains tpy, are considered. The normalized absorption spectra of $Ru^{II}(tpy)Os^{II}$ in water along with $Ru^{II}(tpy)Os^{III}$ and $Ru^{II}(tpm)Os^{III}$ in acetonitrile[**] are displayed below in Figure 3-9. Although the absorption spectra are displayed in

[**]The samples arrived as salts with either a potassium counter ion or a TPP counter ion; potassium salts were water soluble but had limited solubility in acetonitrile whereas theTPP salts were soluble in acetonitrile but not soluble in water

different solvents, there is only a small shift observable in the spectra, which seems to indicate that the use of different solvents is justified. Each sample displays a dominant band in the visible region between 400 and 600 nm. The peak absorption in this region for $Ru^{II}(tpm)Os^{III}$ is blue-shifted relative to the tpy-containing complexes. This blue shift could be the result of the tpm ligand being void of the π conjugation that the tpy ligand possesses. As stated in Chapter 1, the bpy ligand is parallel to the intermetallic axis in tpy- containing complexes, whereas the methyl groups of tpm-containing complexes distort the bpy ligand from planarity.[56] It is believed that this change in geometry may induce more substantial coupling between the metal centers. This observation could explain the difference in band shape of the MLCT transition $Ru^{II}(tpm)Os^{III}$ relative to the shapes of the MLCT bands in dimers $Ru^{II}(tpy)Os^{II}$ and $Ru^{II}(tpy)Os^{III}$. Extended π conjugation in the tpy complexes leads to a red shift of the electronic absorption spectrum, which is what is observed in this case, as compounds $Ru^{II}(tpy)Os^{III}$ and $Ru^{II}(tpm)Os^{III}$ differ only in the terminal ligand.

In order to assess the role of the oxidation state of osmium (OsII vs. OsIII), the electronic absorption spectrum of $Ru^{II}(tpy)Os^{II}$ (dotted line in Figure 3-9), which is the only complex in the present study with osmium in the +2 oxidation state, is compared to the absorption spectra $Ru^{II}(tpy)Os^{III}$ and $Ru^{II}(tpm)Os^{III}$ (Figure 3-9, red dashed and solid black respectively), both containing osmium in the +3 oxidation state. The most obvious difference in the spectra is the presence of an absorption band at wavelengths greater than 600 nm in $Ru^{II}(tpy)Os^{III}$ and $Ru^{II}(tpm)Os^{III}$ that is absent in $Ru^{II}(tpy)Os^{II}$. This because the d^5 osmium centers in $Ru^{II}(tpy)Os^{III}$ and $Ru^{II}(tpm)Os^{III}$ contain a half filled orbital in the highest occupied molecular orbital that can accept the electron, whereas

the d^6 osmium canter in $Ru^{II}(tpy)Os^{III}$has a completely filled orbital which is unable to accept electrons.

Analysis of the MMCT band reveals information about the electronic coupling (V) and the reorganization energy (λ). According to Hush [57, 58]

$$V = \frac{2.05 \times 10^{-2}}{R} \cdot \sqrt{\varepsilon_{max} \nu_{max} \Delta\nu_{1/2}} \qquad (3\text{-}1)$$

where ε_{max} is the maximum molar absorptivity of the band, ν_{max} is the frequency that ε_{max} occurs, $\Delta\nu_{1/2}$ is the bandwidth at half height, and R is the distance between the metal centers. From the absorption spectrum of $Ru^{II}(tpy)Os^{III}$, we can assign ε_{max} = 2135 $M^{-1}cm^{-1}$, ν_{max}= 14450, and $\Delta\nu_{1/2}$=4901 cm^{-1}, resulting in V=1594 cm^{-1}. When V=0, the complex is assigned to class I. When V= $\nu_{max}/2$, the complex is assigned to class III. As neither of these holds true for $Ru^{II}(tpy)Os^{III}$, it is assigned to class II. For an asymmetric complexes like $Ru^{II}(tpy)Os^{III}$, the reorganization energy can be determined from the following equation[39]

$$E_{op} = \Delta G^{\circ} + \lambda \qquad (3\text{-}2)$$

where $E_{op}=\nu_{max}$. The ΔG^{o} term can be estimated from the difference in redox potentials of the two metal centers. The redox potential for $[Os(CN)_6]^{3+}$ is 0.19 V [59] and 1.07 V for $[Ru(bpy)(tpy)(CN)]^{2+}$, [60] resulting in ΔG^{o} equal to -0.86 V, which corresponds to 6932 cm^{-1}. From Equation 3-2, the reorganizational energy is approximated to be 7518 cm^{-1}. Due to instrument constraints, $\Delta\nu_{1/2}$ could not be determined for $Ru^{II}(tpm)Os^{III}$, so the Hush analysis of this complex could not be done at the time.

The transient absorption spectra of Ru(II)(bpy)(tpy)CN and In Ru^{II}(tpy)Os^{II} both exhibit a bleach band in the visible region and excited state absorption in the near UV region. Excitation of Ru^{II}(tpy)Os^{II} at 435 nm does not seem to differ significantly compared to excitation at 480 nm in terms of the positions and widths of the bands. The same observation seems true when comparing the excitation of Ru(II)(bpy)(tpy)CN at 460 nm and 435 nm. However, the transient absorption spectra of Ru^{II}(tpy)Os^{II} is different than that of Ru(II)(bpy)(tpy)CN. In Ru^{II}(tpy)Os^{II}, the presence of a *d-d* metal centered (MC) low lying excited state is possible. This state could explain:

(1) The decrease in luminescence intensity relative to the ruthenium monomer luminescence intensity, as seen in Figure 3-5. Luminescence only comes from MLCT and ligand centered (LC) states in these metal complexes, not from MC states.[61] As the MLCT state transfers population to the non-luminescent MC state, the intensity of the detected emission decreases.

(2) The negative signal in the transient absorption spectra of Ru^{II}(tpy)Os^{II} at wavelengths greater than 600 nm that is seen in figures 3-8 and 3-9. The negative signal is absent in Figure 3-6 and Figure 3-7 for the ruthenium monomer. The shoulder seen at long wavelengths in the UV-Vis spectrum of the Ru-Os^{II} dimer (Figure 3-1) is associated with a Laporte-forbidden transition that is allowed due to a departure from centrosymmetry. In octahedral complexes (which are centrosymmetric) a departure from perfect centrosymmetry in the ground state may relax the Laporte selection rule.[46] In other words, a *d-d* transition is not allowed but may happen due to a distortion due to the environment of the complex. In the case of Ru^{II}(tpy)Os^{II} the distortion of the osmium octahedral center could be due to the presence of the other metal center . Thus, in the transient absorption spectra of Ru^{II}(tpy)Os^{II}, an excited state absorption signal is seen (that is not noticed in the ruthenium monomer) at longer wavelengths that is assigned to this *d-d* transition .

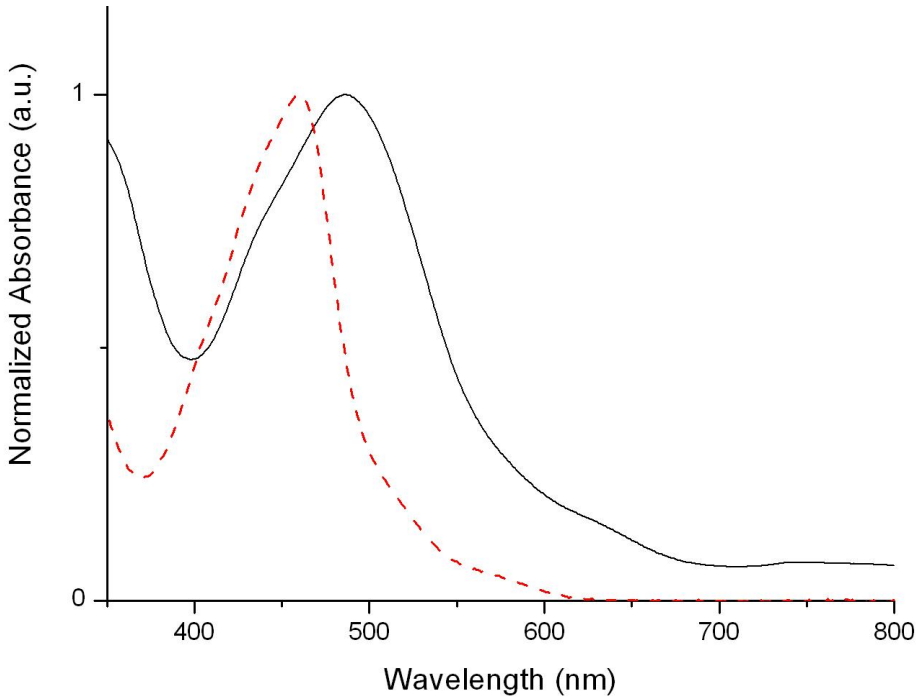

Figure 3-1. Normalized absorption spectra of $Ru^{II}(tpy)Os^{II}$ (black solid line)and [Ru(II)(tpy)(bpy)CN] (red dotted line) in water.

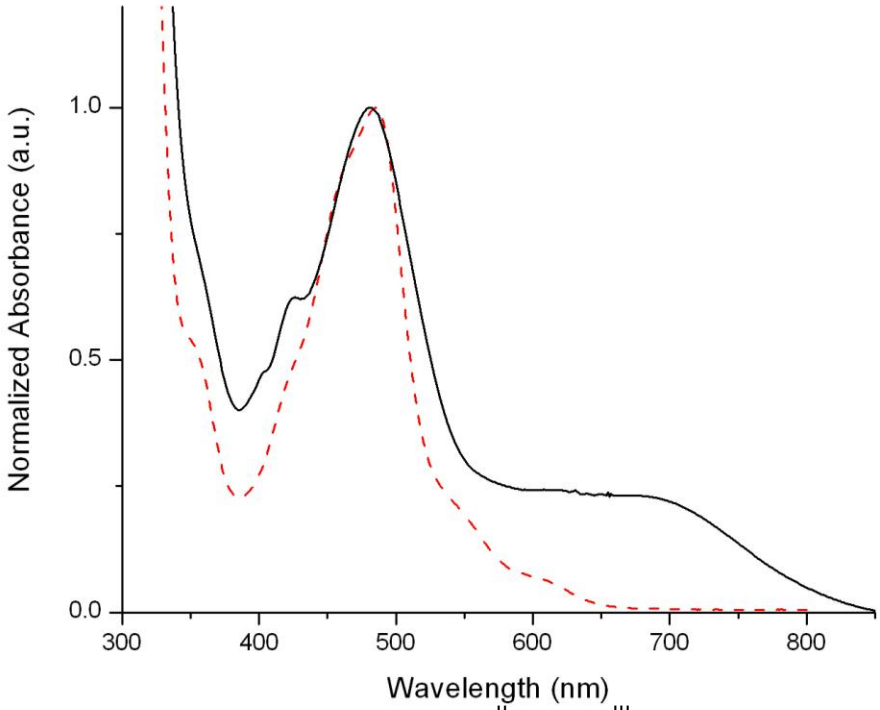

Figure 3-2. Normalized absorption spectra of $Ru^{II}(tpy)Os^{III}$ (black solid line) and the [Ru(tpy)(boy)CN] (red dotted line) in acetonitrile.

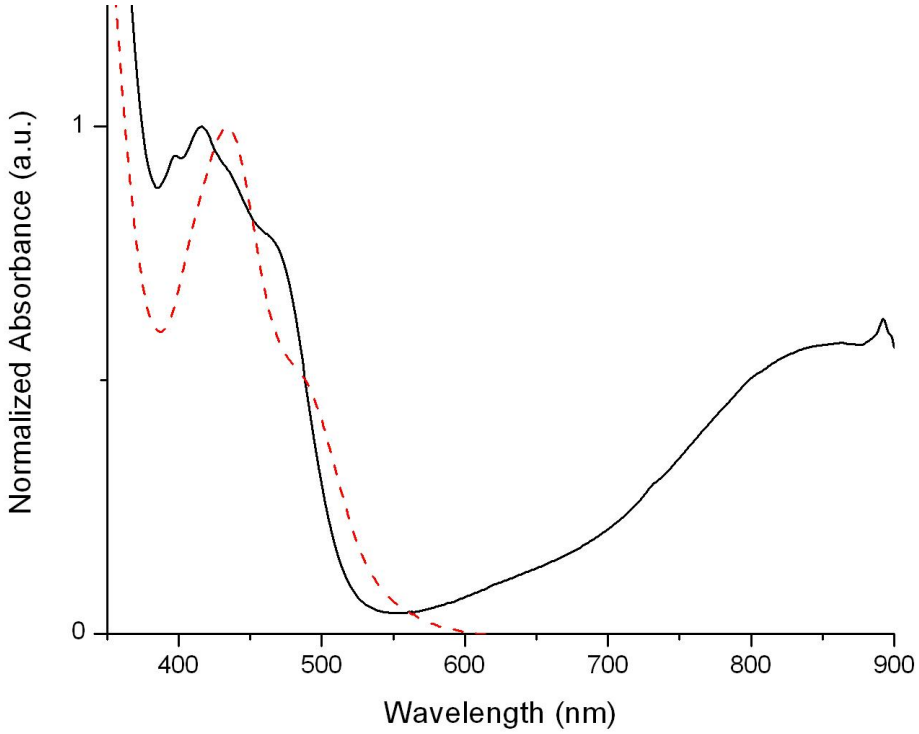

Figure 3-3. Normalized absorption spectra of $Ru^{II}(tpm)Os^{III}$ (black solid line) and [Ru(II)(tpy)(bpy)CN] (red dotted line) in acetonitrile.

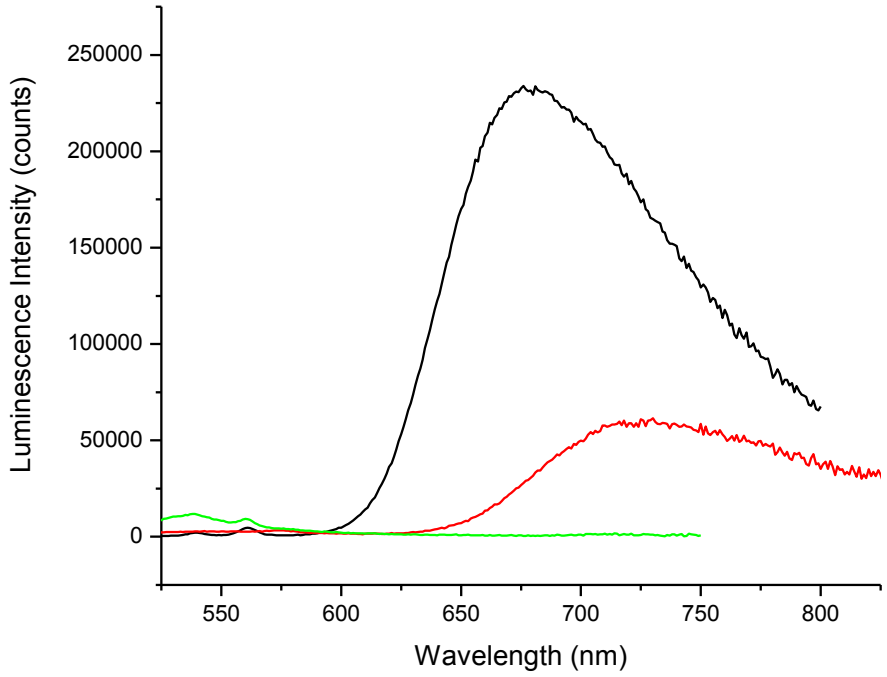

Figure 3-4. Fluorescence emission spectra of [Ru(II)(tpy)(bpy)CN] (black line), $Ru^{II}(tpy)Os^{II}$ (red line) and $Ru^{II}(tpy)Os^{III}$ (green line).

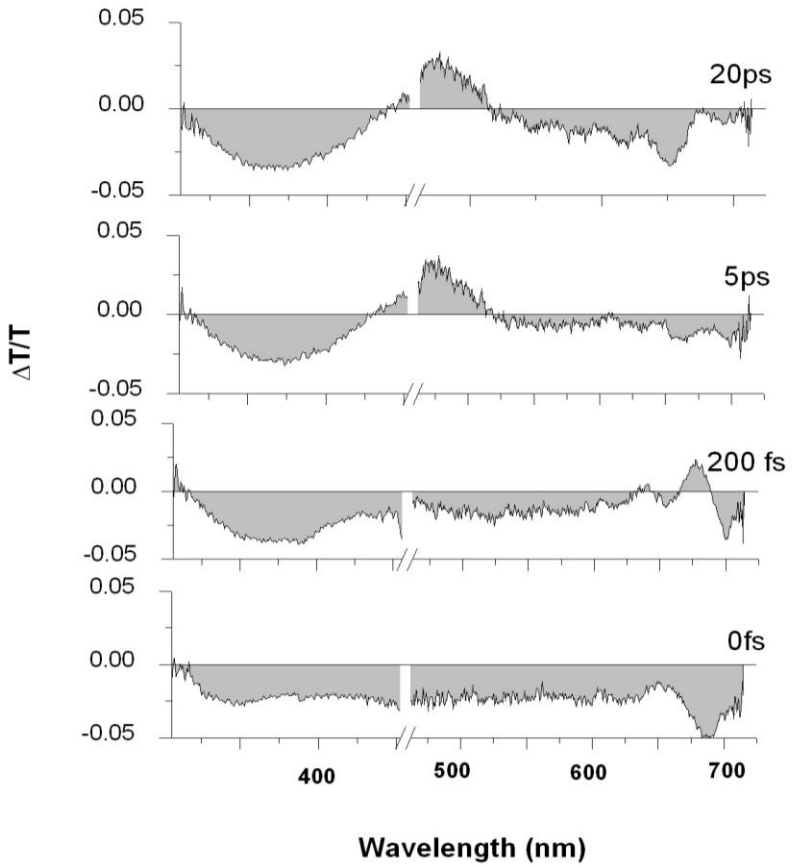

Figure 3-5. Transient absorption spectra of Ru(II)(bpy)(tpy)CN following excitation at 460 nm at different delay times up to 20 ps.

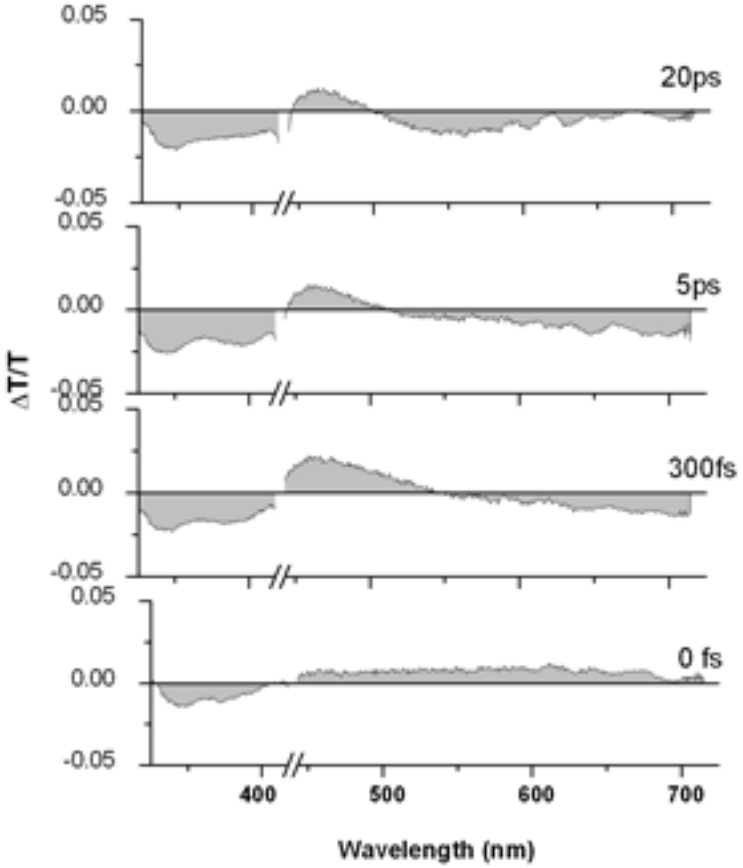

Figure 3-6. Transient absorption spectra of Ru(II)(bpy)(tpy)CN following excitation at 435 nm at different delay times up to 20 ps.

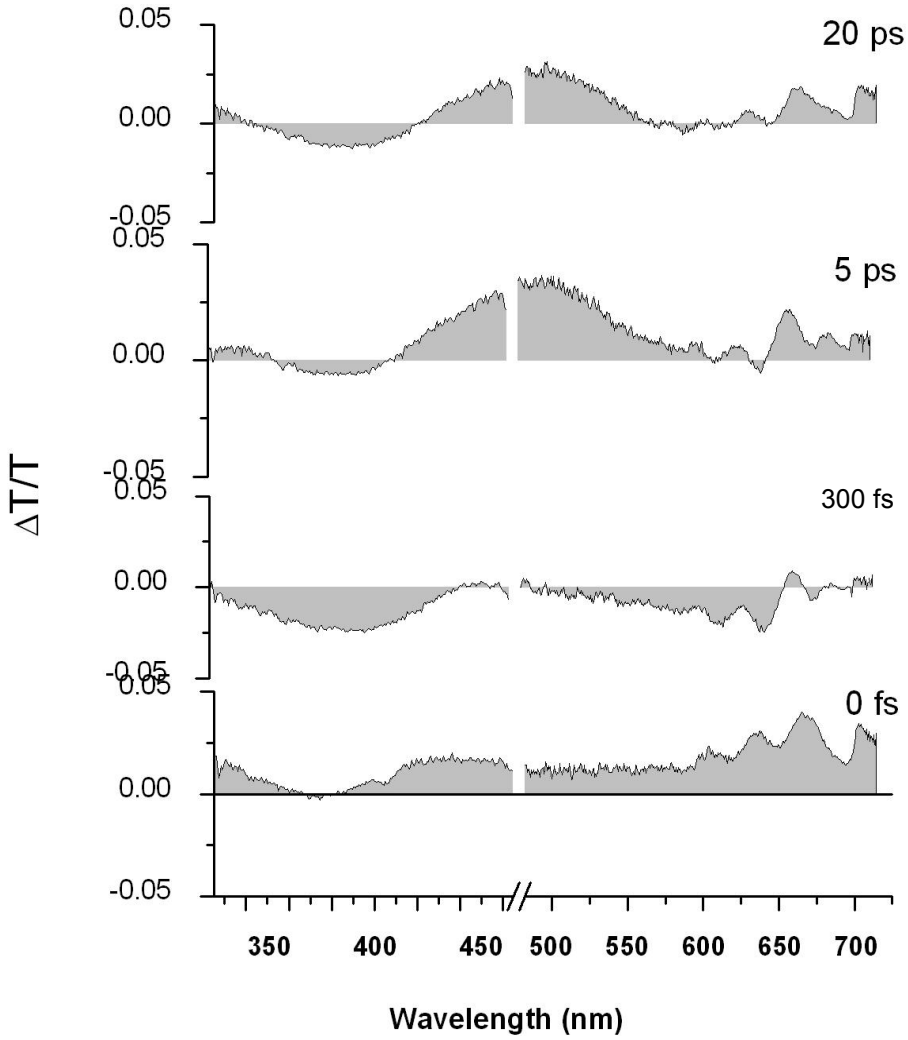

Figure 3-7. Transient absorption spectra of $Ru^{II}(tpy)Os^{II}$ following excitation at 480 nm at different delay times up to 20 ps.

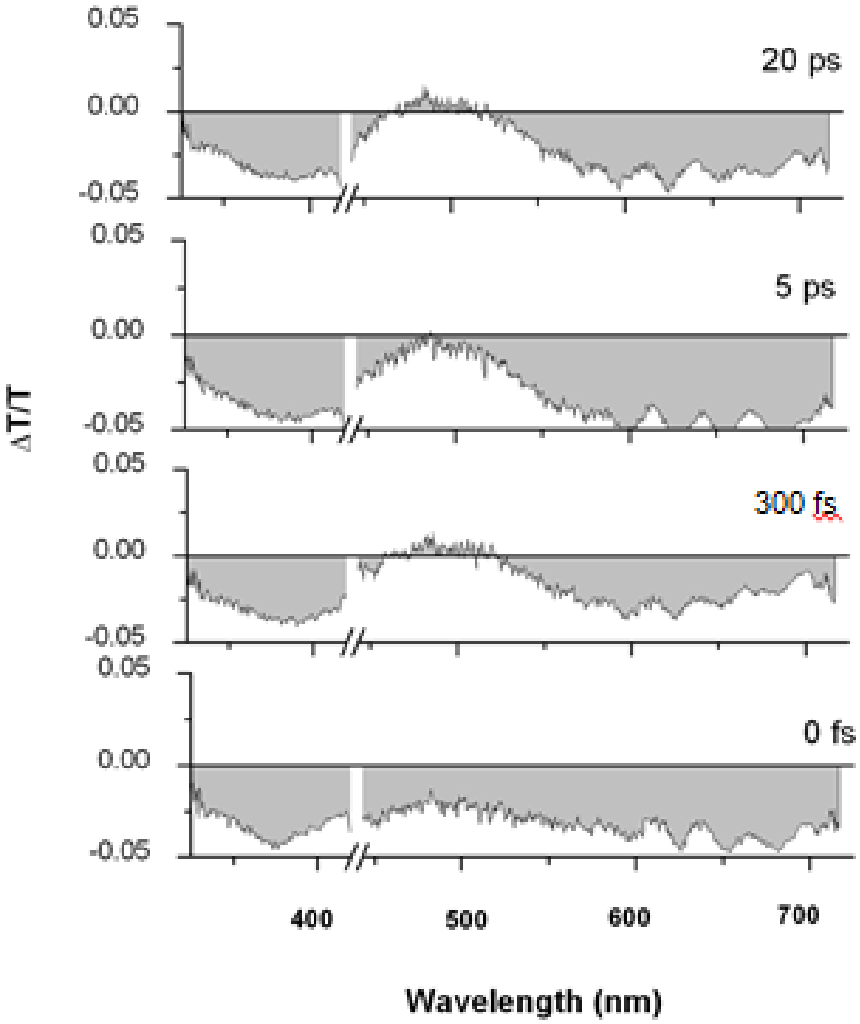

Figure 3-8. Transient absorption spectra of $Ru^{II}(tpy)Os^{II}$ following excitation at 435 nm at different delay times up to 20 ps.

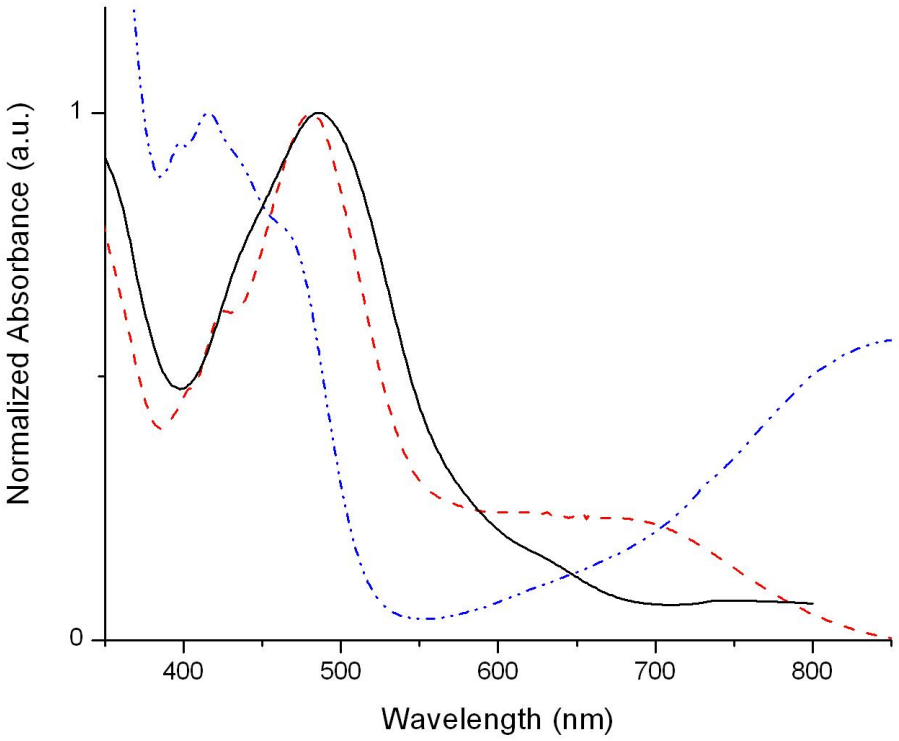

Figure 3-9. Absorption spectra of the binuclear Ru-CN-Os complexes. Black solid line- $Ru^{II}(tpy)Os^{II}$ Red dashed line- $Ru^{II}(tpy)Os^{III}$ Blue dotted line- $Ru^{II}(tpm)Os^{III}$

CHAPTER 4
FUTURE WORK

The data presented here is a preliminary study on the spectroscopic properties of cyanide bridged ruthenium-osmium dimers. However, in order to better understand the excited state dynamics, more work is needed. To understand excited state behavior of these ruthenium-osmium dimers, a study on the properties of a dimer with both ruthenium and osmium in the +2 oxidation state and the tpm ligand would be beneficial. Comparable studies on the $K_2[RuII(tpm)(bpy)(NC)OsII(CN)_5]$ complex[**], should be explored to better understand the effect of geometry on these dimers. To explore metal-to-metal charge transfer, the samples should be excited in the MMCT band. Transient absorption experiments on the mixed valence dimers should be done to determine the dynamics of optical electron transfer upon excitation of the MMCT band.

For the transient absorption experiments, scans proved particularly difficult to obtain with sufficient signal to noise under these experimental conditions. The maximum energy per pulse that was used in these experiments was ~650 nJ. However, many ultrafast transient absorption experiments on transition metal complexes use pulse energies in the microjoule range, from ~2-15 μJ.[37, 62-66] Thus, it is necessary to increase the pulse energy. This is achievable using our current laser system.

An initial characterization of our laser system showed a Spitfire output of 880 μJ per pulse, which was split between OPA I, which is used for fluorescence upconversion experiments, and OPA II, which is used for transient absorption experiments. OPA I was pumped with 480 μJ (55%) and after the phase matching in the BBO crystal had a signal plus idler energy of 111 μJ. OPA II was pumped with 400 μJ (45%) and after the

[**]This complex was not available at the time this work was done

phase matching in the BBO crystal had a signal plus idler energy of 72 μJ measured at a signal wavelength of 1.3 μm. Figure 4-1 is a schematic representing the optics that the pump beam travels through, and Table 4-1 displays pump beam power at various places in the path.

Under the present conditions, signal plus idler (position 3 in Table 4-1) pulse energies of ~64 μJ are achievable. By using a different beamsplitter, such that OPA II is pumped by 55% of the Spitfire output, yielding pulse energies of 450 μJ, the energy at position 3 should increase to ~72 μJ. From Table 4-1, we see that the power following the periscope and second harmonic generation (SHG) (position 4 in Table 4-1) decreases from 60 mW to 15 mW. The SHG crystal used is a BBO type I crystal with a thickness of 0.7 mm. The use of a thicker crystal in SHG has been shown to increase average power by ~ 30% from 0.7 mm to 1 mm.[67] Therefore, by switching the SHG crystal to a 1 mm thick BBO crystal, the power at position 4 in Figure 4-1 should increase from 15 mW to roughly 19 mW. These power increases should result in microjoule pulses for photoexcitation.

In addition to the poor signal to noise obtained due to insufficient pump power, there was also a shift of the baseline of the transients at different times. When the data from Figure 3-7 in the previous chapter is shown in Figure 4-2 below, the effect is more clearly presented. The transients at different probe delays are presented on the same plot, and it is seen that there is a “random” shift of the baseline for each of the delay. In Figure 4-3, a kinetic trace is shown, plotting $\Delta T/T$ at one wavelength as a function of time. In this figure, the sample is excited at 480 nm and probed at 460 nm. The trace is

much too noisy to be fit with a sum of exponentials. These observations seem to be attributed to a wobble caused by the rotation of the calcium fluoride window.

The calcium fluoride window is housed in a home built rotating cell. The wobble, therefore, should be able to be circumvented by designing a new rotating cell as the one presently used may simply have worn parts. Another option would be to generate the supercontinuum using the 790 nm beam focused on a cell with water.[68] White light generation by this method would not require rotation.

To get better time resolution, the duration of the pump beam should be shorter. This is possible through the implementation of a prism compressor to compensate for group velocity dispersion (GVD). GVD is a result of different frequencies of light travel through media at different velocities. Thus, as light passes through optics, the pulses experience broadening. The introduction of negative GVD via a prism pair compensates for the pulse broadening, resulting in a shorter pulse. A pair of prisms set to Brewster's angle can be used to compensate for the difference in velocity, and is shown below in Figure 4-4. After interacting with the first prism, the light is dispersed into individual wavelengths and after the second prism, the light travels parallel to a retroreflector, which sends the parallel beam back along the path. As the red frequencies travel faster than the blue frequencies, the prisms are set such that the red components will traverse more glass from the prism than the blue components.

The prism compressor described here has been used previously in our lab, but is no longer in use because the pulses were compressed only ~20 fs and the retroreflector was believed to be a major source of power loss. The relatively small compression of the pulse has been attributed to the short distance (~25 cm) of the prisms. The prisms

that were used were made of BK7 glass. However, by using TeO_2 crystal prisms, which provides a large GVD constant, the distance of the prisms needed for significant compression can be reduced significantly.[69]

In summary, preliminary data from spectroscopic investigations of ruthenium-osmium binuclear complexes were presented. From the UV-Vis absorption data, the complexes with the osmium +3 oxidation state show a metal-to-metal charge transfer transition that is not seen in the osmium +2 complex. The complex with the tpm ligand shows an absorption spectrum that has a different band shape than the tpy ligand complexes, attributed to a steric effect due to the methyl groups on the tpm ligand. The fluorescence emission spectra show reduced intensity for the binuclear complex with osmium in the +2 oxidation state, and negligible intensity for the complexes containing Os(III). Transient absorption data of the ruthenium monomer and $Ru^{II}(tpy)Os^{II}$ indicate that the lowest MLCT state is formed within 500 fs. A possible low-lying MC state is present in $Ru^{II}(tpy)Os^{II}$. In order to get better signal to noise, the pulse energy must be increased, and the wobble from the white light needs to stop.

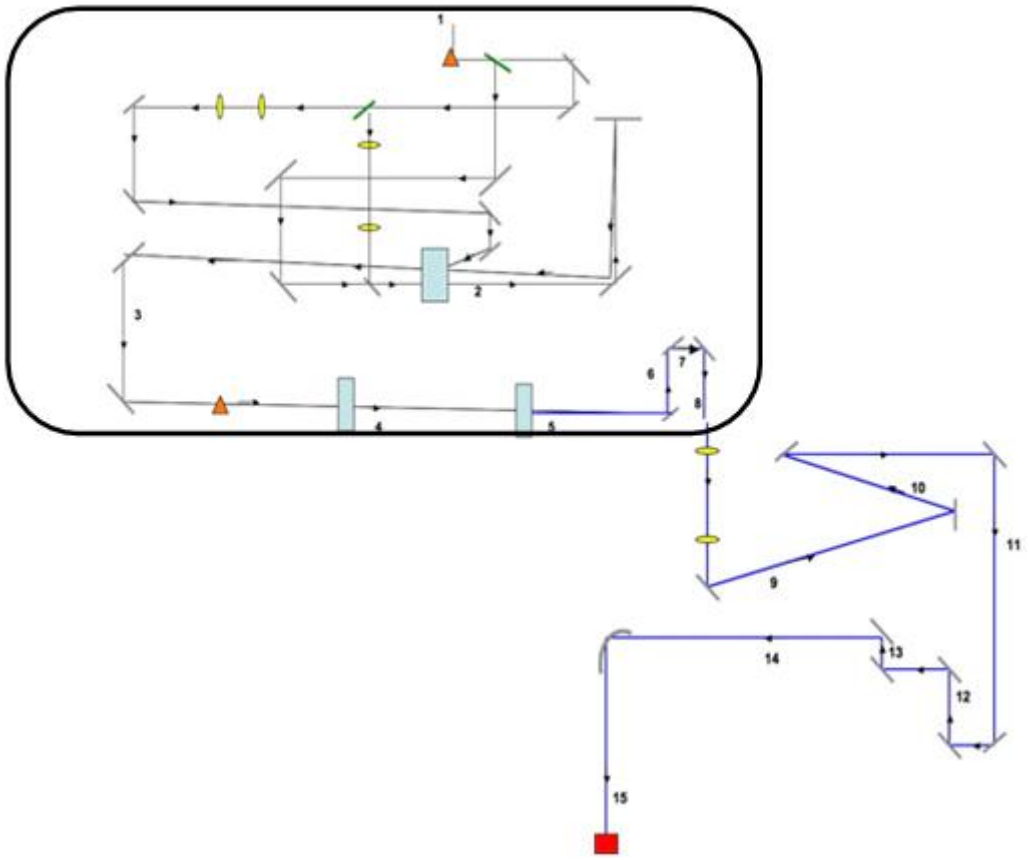

Figure 4-1. Diagram of the optics the pump beam goes through. Grey lines represent mirrors (curved grey line is parabolic mirror), yellow ovals represent lenses, orange triangles represent periscopes, blue boxes represent BBO crystals, and the red square is the sample. The optics within the black rounded rectangle are enclosed by the OPA.

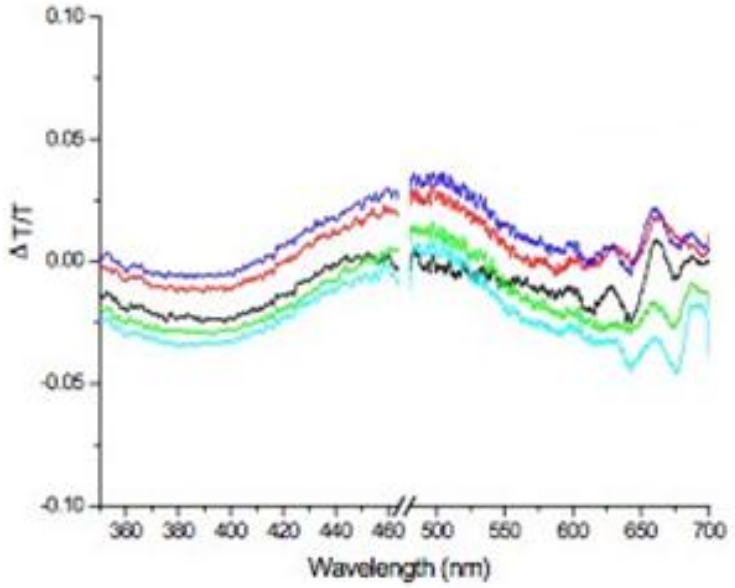

Figure 4-2. Transient absorption spectra of $Ru^{II}(tpy)Os^{II}$ at different delay times following excitation at 480 nm. Black line: 500 fs; Red line: 1 ps; Green line: 5 ps; Blue line: 10 ps; Teal line: 20 ps.

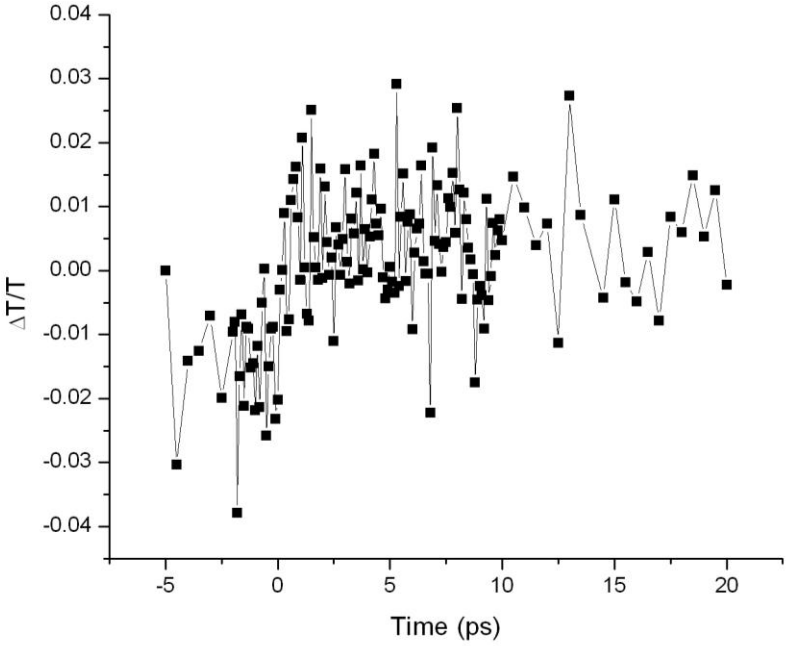

Figure 4-3. Kinetic trace of $Ru^{II}(tpy)Os^{II}$ after photoexcitation at 480 nm, probed at 460 nm.

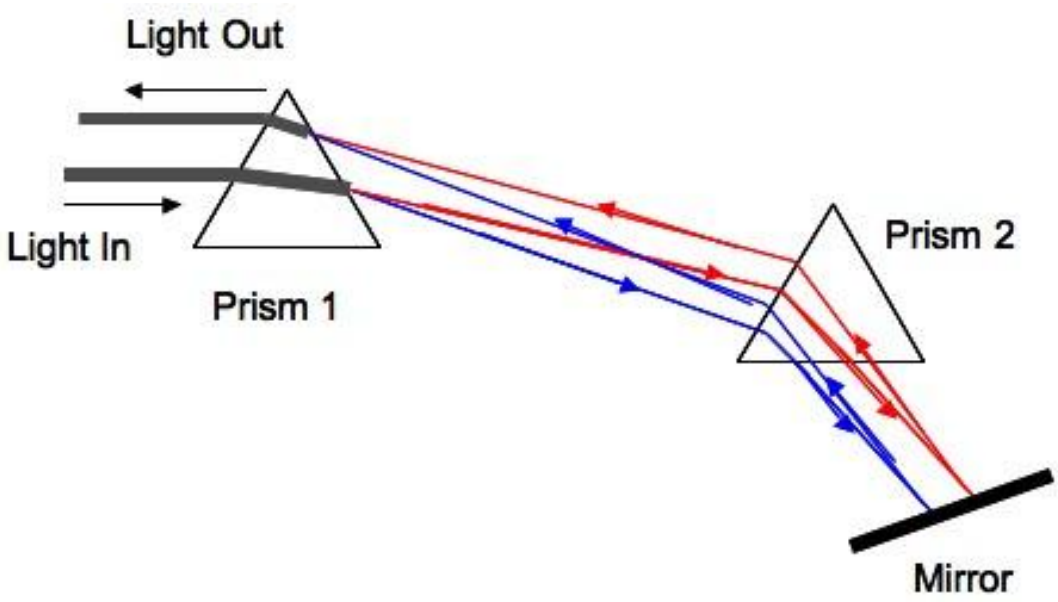

Figure 4-4. Prism compressor schematic

Table 4-1. Pump beam power at different positions in the pump beam path

Position	Power (mW)
1	400
2	40
3	64
4	15
5	14.6
6	1.70
7	1.63
8	1.57
9	1.17
10	1.15
11	1.13
12	0.690
13	0.680
14	0.660
15	0.590

LIST OF REFERENCES

1. Riley, D., The Coming Energy Crisis. *Infinite Energy* 2000.

2. International Energy Outlook 2010. In Energy, D. o., Ed. 2010.

3. Inventory of U.S. Greenhouse Gas Emissions and Sinks: 1990-1998. In Agency, E. P., Ed. 2000.

4. Hermann, W. A., Quantifying global exergy resources. *Energy* **2006,** 31, 1685.

5. Papageorgiou, G. C.; Govindjee, *Chlorophyll A fluorescence: a signature of photosynthesis*. Springer: 2004; p 818.

6. Abrahamsson, M. L. A.; Baudin, H.; Tran, A.; Philouze, C.; Berg, K.; Hammarstrom, L., Ruthenium−Manganese Complexes for Artificial Photosynthesis: Factors Controlling Intramolecular Electron Transfer and Excited-State Quenching Reactions. *Inorganic Chemistry* **2002,** 41, 1534.

7. Gratzel, M., Dye-sensitized solar cells. *Journal of Photochemistry and Photobiology C: Photochemistry Reviews* **2003,** 4, 145.

8. Anscombe, N., Solar cells that mimic plants. *Nature Photonics* **2011,** 5, 266.

9. Meyer, T. J., Chemical approaches to artificial photosynthesis. *Accounts of Chemical Research* **1989,** 22, 163.

10. Balzani, V.; Campagna, S.; Denti, G., Harvesting sunlight by artificial supramolecular antennae. *Solar Energy and Solar Cells* **1995,** 38, 159.

11. Polo, A. S.; Itokazu, M. K.; Iha, N. Y. M., Metal complex sensitizers in dye-sensitized solar cells. *Coordination Chemistry Reviews* **2004,** 248, 1343.

12. Bingwen, J.; Manhua, Z.; Tao, S., Advances in dye-sensitized solar cell. *Chinese Science Bulletin* **1997,** 42, 1937.

13. Juris, A.; Balzani, V.; Barigelletti, F.; Campagna, S.; Belser, P.; Von Zalersky, A., Ru(II) polypyridine complexes: photophysics, photochemistry, eletrochemistry, and chemiluminescence. *Coordination Chemistry Reviews* **1988,** 84, 85.

14. Yeh, A. T.; Shank, C. V.; McCusker, J. K. S., Ultrafast Electron Localization Dynamics Following Photo-Induced Charge Transfer. *Science* **2000,** 289, 935.

15. Damrauer, N. H.; Cerullo, G.; Yeh, A.; Boussie, T. R.; Shank, C. V.; McCusker, J. K., Femtosecond Dynamics of Excited-State Evolution in [Ru(bpy)3]2+. *Science* **1997,** 275, 54.

16. Demas, J. N.; Crosby, G. A., Quantum efficiencies on transition metal complexes. II. Charge-transfer luminescence. *Journal of the American Chemical Society* **1971,** 93, 2841.

17. Balzani, V.; Campagna, S.; Denti, G.; Juris, A.; Venturi, M., Designing Dendrimers Based on Transition-Metal Complexes. Light-Harvesting Properties and Predetermined Redox Patterns. *Accounts of Chemical Research* **1998,** 31, 26.

18. Balzani, V.; Juris, A.; Venturi, M., Luminescenet and Redox-Active Polynuclear Transition Metal Complexes. *Chemical Reviews* **1996,** 96, 759.

19. Anderson, P. A.; Strouse, G. F.; Treadway, J. A.; Keene, F. R.; Meyer, T. J., Black MLCT Absorbers. *Inorganic Chemistry* **1994,** 33, 3863.

20. Arana**,** C. R.; Abrufia**,** H. D., Monomeric and oligomeric complexes of ruthenium and osmium with tetra-2-pyridyl-1,4-pyrazine (TPPZ). *Inorganic Chemistry* **1993,** 32, 194.

21. Collin, J. P.; Guillerez, S.; Sauvage, J. P.; Barigelletti, F.; De Cola, L.; Flamigni, L.; Balzani, V., Photoinduced processes in dyads and triads containing a ruthenium(II)-bis(terpyridine) photosensitizer covalently linked to electron donor and acceptor groups. *Inorganic Chemistry* **1991,** 30, 4230.

22. Kober, E. M.; Marshall, J. L.; Dressick, W. J.; Sullivan, B. P.; Meyer, T. J., Synthetic control of excited states. Nonchromophoric ligand variations in polypyridyl complexes of osmium(II). Inorganic Chemistry 1985, 24, 2755.

23. Schering, T.; Kaim, W.; Olabe, J. A.; Parise, A. R.; Fiedler, J., The valence-localized decacyanodiruthenium(III,II) analogue of the Creutz–Taube ion. Completing the full d^5/d^6 triad $[(NC)_5M(\mu\text{-}pz)M(CN)_5]^{5-}$, M=Fe,Ru,Os; pz=pyrazine. *Inorganica Chimicia Acta* **2000,** 300-302, 125.

24. Song**,** X.; Y**.** Lei; Wallendal**,** S. V.; Perkovic**,** M. W.; Jackman**,** D. C.; J. F. Endicott; D. P. Rillema**,** J., Photoinduced electron-transfer processes involving covalently linked ruthenium and cobalt polypyridyl complexes: comparison of electronic coupling in bridged and nonbridged ruthenium and cobalt complexes. *Journal of Physical Chemistry* **1993,** 97, 3225.

25. Strouse, G. F.; Anderson, P. A.; Schoonover, J. R.; Meyer, T. J.; Keene, F. R., Synthesis of polypyridyl complexes of ruthenium(II) containing three different bidentate ligands. *Inorganic Chemistry* **1992,** 31, 3004.

26. Winkler, J. R.; Netzel, T. L.; Okumura, M.; Sutin, J., Direct observation of metal-to-ligand charge-transfer (MLCT) excited states of pentaammineruthenium(II) complexes. *Journal of the American Chemical Society* **1987,** 109, 2381.

27. Yoshimura**,** A.; Nozaki**,** K.; Ikeda**,** N.; Ohno**,** T., Temperature-Dependent Rates of Electron Transfers and Intersystem Crossing on the Laser Excitation of Ligand-Bridged Ru(II) and Co(III) Compounds. *Journal of Physical Chemistry* **1996,** 100, 1630.

28. Scandola, F.; Bignozzi, C. A.; Chiorboli, C.; Rampi, M. A., Intramolecular energy transfer in Ru(II)-Ru(II) and Ru(II)-Cr(III) polynuclear complexes. *Coordination Chemistry Reviews* **1990,** 97, 299.

29. Sears, R. B.; Joyce, L. E.; Turro, C., Electronic Tuning of Ruthenium Complexes by 8-Quinolate Ligands. *Photochemistry and Photobiology* **2010,** 86, 1230.

30. Belser, P.; Bernhardt, S.; Blum, C.; Beyeler, A.; DeCola, L.; Balzani, V., Molecular architecture in the field of photonic devices. *Coordination Chemistry Reviews* **1990,** 190, 155.

31. Schlicke, B.; Belser, P.; De Cola, L.; Sabbioni, E.; Balzani, V., Photonic Wires of Nanometric Dimensions. Electronic Energy Transfer in Rigid Rodlike $Ru(bpy)_3^{2+}$-$(ph)_n$-$Os(bpy)_3^{2+}$ Compounds (ph = 1,4-Phenylene; *n* = 3, 5, 7). *Journal of the American Chemical Society* **1999,** 121, 4207.

32. Moore, K. J.; Lee, L.; Figard, J. E.; Gelroth, J.; Stinson, A. J.; Petersen, J. D., Photochemistry of mixed-metal bimetallic complexes containing pentaammineruthenium(II) metal centers. Evidence for some intramolecular energy-transfer reactions. *Journal of the American Chemical Society* **1983,** 105, 2274.

33. Guldi, D. M.; Maggini, M.; Menna, E.; Roffia, S., A Photosensitizer Dinuclear Ruthenium Complex: Intramolecular Energy Transfer to a Covalently Linked Fullerene Acceptor. *Chemistry-A European Journal* **2001,** 7, 1597.

34. Camera, S. G.; Toma, H. E., Photophysical behavior of molecular dyads and triad comprising tris(bipyrazine)ruthenium^{II}, bis(bipyridine)chlororuthenium^{II} and pentacyanoferrate^{II} complexes. **2002,** 151, 57.

35. Barigelletti, F.; L.Flamigni; V.Balzani; J.P.Collin; J.P.Sauvage; A.Sour; E.C.Constable; Thompson, A. M. W. C., Rigid Rod-Like Dinuclear Ru(II)/Os(II) Terpyridine-Type Complexes. Electrochemical Behavior, Absorption Spectra, Luminescence Properties, and Electronic Energy Transfer through Phenylene Bridges. *Journal of the American Chemical Society* **1994,** 116, 7692.

36. Indelli**,** M. T.; Scandola**,** F., J.-P. C.; Sauvage**,** J.-P.; Sour**,** A., Photoinduced Electron and Energy Transfer in Rigidly Bridged Ru(II)−Rh(III) Binuclear Complexes. *Inorganic Chemistry* **1996,** 35, 303.

37. Doorn, S. K.; Dyer, R. B.; Southland, P. O.; Woodruff, W. H., Ultrafast electron transfer and coupled vibrational dynamics in cyanide bridged mixed-valence transition-metal dimers. *Journal of the American Chemical Society* **1993,** 115, 6398.

38. Robin, M. B.; Day, P., Mixed Valence Chemistry-A Survey and Classification. *Advances in Inorganic Chemistry and Radiochemistry* **1967,** 10, 247.

39. Bernhardt, P. V.; Bozoglian, F.; Macpherson, B.; Martinez, M., Molecular mixed-valence cyanide bridged Co^{III}–Fe^{II} complexes. *Coordination Chemistry Reviews* **2005,** 249, 1902.

40. Hoshini, Y., Molecular Design for Long-Range Electronic Communication between Metals. *Platinum Metals Review* **2001,** 45, 2.

41. Curtis, J. C.; Roberts, J. A.; Blackbourn, R. L.; Johnson, C. S.; Hupp, J. T., Solvent-induced and polyether-ligand-induced redox isomerization within an asymmetrically coordinated mixed-valence ion: trans-tetraamminebis(2,2'-bipyridine)(mu.-4-cyanopyridine)chloro(pyridine)diruthenium(4+), trans-(py)(NH3)4Ru(4-NCpy)Ru(2,2'-bpy)2Cl4+. *Inorganic Chemistry* **1991,** 30, 3856.

42. Roberts, J. A.; Bebel, J. C.; Absi, M. L.; Hupp, J. T., Selective-solvation-induced intramolecular electron transfer: time resolution via pulsed accelerated flow spectrophotometry. *Journal of the American Chemical Society* **1992,** 114, 7957.

43. Wolpher, H.; Sinha, S.; Pan, J.; Johansson, A.; Lundqvist, A.; Persson, P.; Lomoth, R.; Bergquist, J.; Sun, L.; Sundstrom, V.; Akermark, B.; Polivka, T., Synthesis and Electron Transfer Studies of Ruthenium−Terpyridine-Based Dyads Attached to Nanostructured TiO_2. *Inorganic Chemistry* **2007,** 46, 638.

44. Videla**,** M.; Jacinto**,** J.; Baggio**,** R.; Garland**,** M.; Singh**,** P.; Kaim**,** W.; Slep**,** L. D.; Olabe**,** J., New Ruthenium Nitrosyl Complexes with Tris(1-pyrazolyl)methane (tpm) and 2,2‘-Bipyridine (bpy) Coligands. Structure, Spectroscopy, and Electrophilic and Nucleophilic Reactivities of Bound Nitrosyl. *Inorganic Chemistry* **2006,** 45, 8608.

45. Verdauger, M.; Bleuzen, A.; Marvaud, V.; Vaisserman, J.; Scullier, A.; Train, C.; Gelly, G.; Veillet, P.; Villain, F., Molecules to build solids: high T_C molecule-based magnets by design and recent revival of cyano complexes chemistry. *Coordination Chemistry Reviews* **1999,** 190-192, 1023.

46. Atkins, P.; Overton, T.; Rourke, J.; Weller, M.; Armstrong, M. *Inorganic Chemistry*. 4th ed.; W.H.Freeman: 2006; p 822.

47. Billing, R., Optical and photoinduced electron transfer in ion pairs of coordination compounds. *Coordination Chemistry Reviews* **1997,** 159, 257.

48. Balzani, V.; Juris, A.; Venturi, M.; Campagna, S.; Serroni, S., Luminescenet and Redox-Active Polynuclear Transition Metal Complexes. *Chemical Reviews* **1996,** 96, 759.

49. Li, Y. Electron transport in ferrocenes linked by molecular wires. Georgia Institute of Technology, 2007.

50. Berera, R.; Grondelle, R. v.; Kennis, J. T. M., Ultrafast Transient absorption spectroscopy: principles and application to photosynthetic systems. *Photosynthesis Research* **2009,** 101, 105.

51. Atas, E. Ultrafast time resolved excitation dynamics in conjugated dendrimers. University of Florida, 2006.

52. Albores, P.; Slep, L. D.; Baraldo, L. M.; Baggio, R.; Garland, M.; Rentschler, E., Crystal Structure and Electronic and Magnetic Properties of Hexacyanoosmate(III) . *Inorganic Chemistry* **2006,** 45, 2361.

53. Llobet, A.; Dopplet, P.; Meyer, T. J., Redox properties of aqua complexes of ruthenium(II) containing the tridentate ligands 2,2':6',2"-terpyridine and tris(1-pyrazolyl)methane. *Inorganic Chemistry* **1988,** 27, 514.

54. McCusker, J. K., Femtosecond Absorption Spectroscopy of Transition Metal Charge-Transfer Complexes. *Accounts of Chemical Research* **2003,** 36, 876.

55. Velayudham, M.; Rajagopal, S., Synthesis, characterization and photophysics of bimetallic manganese (I) and ruthenium (II) complexes. *Polyhedron* **2009,** 28, 3043.

56. Gonzalez, V.; Adams, H. A.; Thomas, J. A., A convenient synthetic route to half-sandwich rhodium(III) complexes of the tripodal ligand tris(3,5-dimethylpyrazolyl)methane. *Dalton Transactions* **2005**, 110.

57. Hush, N. H., Homogeneous and heterogeneous optical and thermal electron transfer. *Electrochimica Acta* **1968,** 13, 1005.

58. Altabef, A. B.; Galla, S. B. R. d.; Folquer, M. E.; Katz, N. E., Dinuclear complexes of (2,2′-bipyridine)(2,2′:6′,2"-terpyridine)-ruthenium(II) bonded through cyanide to pentaammineruthenium(II/III) groups. *Transition Metal Chemistry* **1993,** 18, 319.

59. Srnec, M.; Chalupsky, J.; Fojta, M.; Zendlova, L.; Hocek, M.; Kyvala, M.; Rulisek, L., Effect of Spin−Orbit Coupling on Reduction Potentials of Octahedral Ruthenium(II/III) and Osmium(II/III) Complexes. *Journal of the American Chemical Society* **2008,** 130, 10947.

60. Ponce, A.; Bachrach, M.; Farmer, P.; Winkler, J., Intramolecular electron transfer in cyanide-bridged ruthenium dimers. *Inorganica Chimicia Acta* **1996,** 243, 135.

61. Lakowicz, J. R., *Principles of Fluorescence Spectroscopy*. 2nd ed.; Springer: 1999; p 725.

62. Abbott, L.; Arnold, C.; Ye, T.-Q.; Gordon, K. C.; Perutz, R.; Hester, R. E.; Moore, J. N., Ultrafast Time-Resolved UV−Visible and Infrared Absorption Spectroscopy of Binuclear Rhenium(I) Polypyridyl Complexes in Solution. *Journal of Physical Chemistry A* **1998,** 102, 1252.

63. Baudin, H.; Davidsson, J.; Serroni, S.; Juris, A.; Balzani, V.; Campagna, S.; Hammarstrom, L., Ultrafast Energy Transfer in Binuclear Ruthenium−Osmium Complexes as Models for Light-harvesting Antennas. *Journal of Physical Chemistry A* **2002,** 106, 4312.

64. Damrauer, N. H.; McCusker, J. K., Ultrafast Dynamics in the Metal-to-Ligand Charge Transfer Excited-State Evolution of [Ru(4,4′-diphenyl-2,2′-bipyridine)3]2+. *Journal of Physical Chemistry A* **1999,** 103, 8440.

65. Kuciauskas, D.; Monat, J. E.; Villahermosa, R.; Gray, H.; Lewis, N. S.; McCusker, J. K., Transient Absorption Spectroscopy of Ruthenium and Osmium Polypyridyl Complexes Adsorbed onto Nanocrystalline TiO_2 Photoelectrodes. *Journal of Physical Chemistry B.* **2002,** 106, 9347.

66. McFarland, S. A.; Cheng, K. A. W. Y.; Lee, F. S.; Cozens, F. L.; Schepp, N. P., Nonthermalized excited states in Ru(II) polypyridyl complexes probed by ultrafast transient absorption spectroscopy with high photon energy excitation. *Canadian Journal of Chemistry* **2008,** 86, 1118.

67. Ashworth, S. H.; Joschko, M.; Woerner, M.; Reidle, E.; Elasasser, T., Generation of 16-fs pulses at 425 nm by extracavity frequency doubling of a mode-locked Ti:sapphire laser. *Optics Letters* **1995,** 20, 2120.

68. Kolesik, M.; Katona, G.; Moloney, J. V.; Wright, E. M., Theory and simulation of supercontinuum generation in transparent bulk media. *Applied Physics B.* **2003,** 77, 185.

69. Nakazawa, M.; Nakashima, T.; Kubota, H.; Seikai, S., Efficient optical pulse compression using a pair of Brewster-angled TeO2 crystal prisms. *Journal of the Optical Society of America* **1988,** 5, 215.

BIOGRAPHICAL SKETCH

Jaired Elliott Tate was born in Atlanta, GA in 1983 to James and Jean Tate. Upon his graduation from Westlake High School in 2001, he enrolled at Florida A&M University in Tallahassee, FL. Initially enrolled as a biology major, he switched his major to chemistry during his junior year. In 2005, he graduated with a B.S. degree in chemistry. Following this, he enrolled in graduate school at Florida A&M University, working in the lab of Dr. Maurice Edington and received a M.S. degree in chemistry in 2008. In the fall of 2008, he began his graduate studies at the University of Florida where he joined the research group of Dr. Valeria Kleiman.

He currently resides in Gainesville, FL with his wife, Tia, and his son, Jaired, Jr. He hopes to remain at UF and earn a Ph.D. in chemistry. His career goal is to teach at a small university and eventually get an administrative position.